Novel, Oxygen-Deficient $n = 3$ RP-Member $Sr_3NdFe_3O_{9-\delta}$ and Its Topotactic Derivatives

D. Pelloquin,* J. Hadermann,† M. Giot, V. Caignaert, C. Michel, M. Hervieu, and B. Raveau

Laboratoire CRISMAT-ENSICAEN, UMR6508, 6, Bd du Maréchal Juin, 14050 Caen Cedex, France

Received October 15, 2003. Revised Manuscript Received February 5, 2004

The stabilization of the $n = 3$ member of the Ruddlesden−Popper series has been investigated in the Sr−Nd−Fe−O system. A new series of phases closely derived from RP-type structures has been synthesized and characterized by X-ray diffraction and electron microscopy. The control of the oxygen stoichiometry first allowed us to isolate a new highly oxygen deficient, layered oxide, $Sr_3NdFe_3O_{9-\delta}$. The structural analysis has revealed that this oxide crystallizes in an orthorhombic lattice ($a_p\sqrt{2} \times a_p\sqrt{2} \times 28$ Å), distorted with regard to the ideal *I*-type symmetry of the RP-type structures. Interestingly, this oxygen-deficient $n = 3$ RP-member reacts at room temperature with ambient moisture to transform into a hydrated oxyhydroxide, $Sr_3NdFe_3O_{7.5}(OH)_2{\cdot}H_2O$. This second phase can be dehydrated topotactically in two steps by heating to 400 °C, leading to $Sr_3NdFe_3O_{7.5}(OH)_2$ and then $Sr_3NdFe_3O_{8.5+\delta}$, respectively. The reversible character of these hydration/hydrolysis reactions is also demonstrated.

Introduction

Titanates of the Ruddlesden and Popper series $Sr_{n+1}Ti_nO_{3n+1}$[1] represent the first members of a huge family of layered oxides that are closely related to perovskite. Starting from these compounds, whose structure is built up from the intergrowth of a single rock salt layer [SrO] with multiple perovskite layers $[SrTiO_3]_n$, new structural series were generated by increasing the multiplicity of the rock salt layers, especially introducing Bi, Tl, Pb, and Hg, or by creating ordered oxygen deficiency within the multiple perovskite layers. This is exemplified by the numerous high T_c superconducting cuprates that were discovered these last 15 years.[2−3] Interest for the RP structure was also renewed with the discovery of colossal magnetoresistance in the layered manganites.[4−5] Several bismuth-, thallium-, and lead-based cobaltites[6−9] and ferrites[10−16] and a chromium-based oxide, $Sr_4Cr_{2.5}O_9$,[11] derived from RP-type structures were also isolated.

The existence of the three first members of the RP series $Sr_{n+1}Fe_nO_{3n+1}$,[18−20] all characterized by the presence of Fe^{4+}, makes the system Sr−Fe−O very attractive for the generation of new RP phases. In such a system, the introduction of a lanthanide on the Sr sites or of carbonate groups in the octahedral layers leads to the formation of Fe^{3+} derivatives, as shown by the existence of RP-type oxides in the system $LaSr_3Fe_3O_{10-x}$,[21] with x varying from 0 to 1, and oxycarbonates $Sr_4Fe_{3-x}O_{10-4x}(CO_3)_x$.[22] We have investigated the Sr−Nd−Fe−O system, controlling the oxygen stoichiometry

* Corresponding author. E-mail: denis.pelloquin@ismra.fr.

† Permanent address: EMAT Laboratory, University of Antwerpen-RUCA, Groenenborgerlaan 171, 2020 Antwerpen, Belgium.

(1) Ruddlesden, S. N.; Popper, P. *Acta Crystallogr.* **1957**, *10*, 538; ibid **1958**, *11*, 54.

(2) See for a review, Rao, C. N.; Raveau, B. *Transition Metal Oxides*; Wiley-VCH: New York, 1998.

(3) See for a review, Raveau, B.; Michel, C.; Hervieu, M.; Groult, D. *Crystal Chemistry of High Tc Superconducting Copper Oxides*; Springer Series Materials Science; Springer-Verlag: Berlin, 1991.

(4) Kimura, K.; Hatsuda, K.; Ueno, Y.; Kajimoto, R.; Mochizuki, A.; Yoshizawa, H.; Nagai, T.; Matsui, Y.; Yamazaki, A.; Tokura, Y. *Phys. Rev. B* **2001**, *65*, 20407.

(5) Maignan, A.; Martin, C.; Van Tendeloo, G.; Hervieu, M.; Raveau, B. *J. Mater. Chem.* **1998**, *8*, 2411.

(6) Tarascon, J. M.; Miceli, P. F.; Barboux, P.; Hwang, D. M.; Hull, G. W.; Giroud, M.; Greene, L. H.; Lepage, Y.; McKinnon, W. R.; Tselepis, E.; Pleizier, G.; Eibschutz, M.; Neumann, D. A.; Phyne J. J. *Phys. Rev. B* **1989**, *39*, 11587.

(7) Coutanceau, M.; Dordor, P.; Doumerc, J. P.; Grenier, J. C.; Maestro, P.; Pouchard, M.; Semidubsky, D.; Seguelong, T. *Solid State Commun.* **1995**, *96*, 569.

(8) Groult, D.; Martin, C.; Maignan, A.; Pelloquin, D.; Raveau, B. *Solid State Commun.* **1998**, *105*, 583.

(9) Pelloquin, D.; Masset, C.; Maignan, A.; Hervieu, M.; Michel, C.; Raveau, B. *J. Solid State Chem.* **1999**, *148*, 108.

(10) Pelloquin, D.; Allix, M.; Michel, C.; Hervieu, M.; Raveau, B. *Philos. Mag. B* **2001**, *81* (11), 1669−1685.

(11) Pelloquin, D.; Wahl, A.; Masset, A. C.; Maignan, A.; Michel, C.; et Raveau, B. *J. Solid. State. Chem.* **2000**, *154* (2), 375−383.

(12) . Retoux, R.; Michel, C.; Hervieu, M.; Nguyen, N.; Raveau, B. *Solid State Commun.* **1989**, *69*, 599.

(13) Daniel, Ph.; Barbey, L.; Nguyen, N.; Ducouret, A.; Groult, O.; Raveau, B. *J. Phys. Chem. Solids* **1994**, *55*, 795.

(14) Caignaert, V.; Daniel, Ph.; Nguyen, N.; Groult, O.; Raveau, B. *J. Solid State Chem.* **1994**, *112*, 126.

(15) Hervieu, M.; Pelloquin, D.; Michel, C.; Caldès, M. T.; Raveau, B. *J. Solid State Chem.* **1995**, *118*, 227.

(16) Boullay, Ph.; Domenges, B.; Groult, D.; Raveau, B. *J. Solid State Chem.* **1996**, *124*, 1.

(17) Nguyen, N.; Groult, D.; Caignaert, V.; Ducouret, A.; Raveau, B. *Phys. B, Condens. Matter* **1996**, *228*, 251.

(18) Dann, S. E.; Weller, M. T.; Curie, D. B. *J. Solid State Chem.* **1991**, *92*, 237.

(19) Dann, S. E.; Weller, M. T.; Curie, D. B. *J. Solid State Chem.* **1992**, *97*, 179.

(20) Brisi, C.; Rolando, *Ann. Chim. (Rome)* **1969**, *59*, 385.

(21) Lee, J. Y.; Swinn, J. S.; Ea, P.; Steinfink, H.; Reiff, W. M.; Pei, S.; Jorgensen, J. D. *J. Solid State Chem.* **1993**, *103*, 1.

(22) Bréard, Y.; Michel, C.; Hervieu, M.; Raveau, B. *J. Mater. Chem.* **2000**, *10*, 1043.

10.1021/cm030351n CCC: $27.50 © 2004 American Chemical Society
Published on Web 04/01/2004

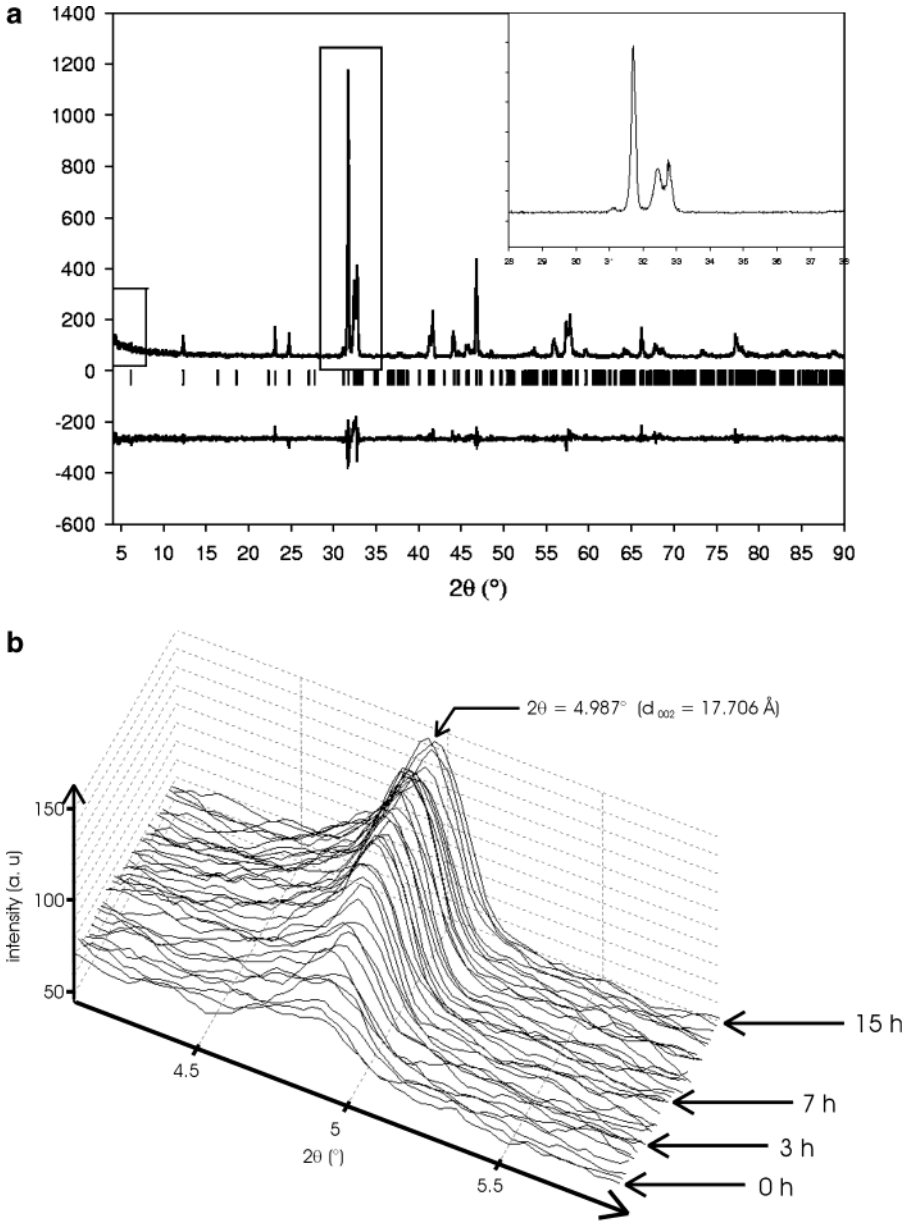

Figure 1. (a) XRD pattern of the as-synthesised $Sr_3NdFe_3O_{8.5}$ recorded at room temperature under N_2 flow. This pattern is indexed in the *Bbm2* space group (5.4 × 5.4 × 28.5 Å^3), while the evolution in air of the sample is shown in part b.

in order to involve divalent iron. We report herein on a highly oxygen deficient, $n = 3$ RP ferrite, with nominal composition $Sr_3NdFe_3O_{8.5}$, showing it is a labile oxide and reacts at room temperature in the presence of H_2O. It topotactically transforms into a layered oxyhydroxide hydrate $Sr_3NdFe_3(OH)_2O_{7.5+\delta}{\cdot}H_2O$. We also demonstrate that this second phase can be dehydrated topotactically by heating to 250 °C, leading first to $Sr_3NdFe_3(OH)_2O_{7.5+\delta}$ and then to $Sr_3NdFe_3O_{8.5+\delta}$. The electron microscopy study allows the cell parameters and symmetry of the metastable phases to be determined and also structural models and mechanisms to be proposed. The reversible character of the hydration/hydrolysis reactions in this system is also demonstrated.

Experimental Section

The exploration of the system $Sr_3NdFe_3O_{10-x}$ oxide was carried out in evacuated sealed tubes, by solid-state route, starting from adequate mixtures of SrO_2, Nd_2O_3, Fe_2O_3 oxides and Fe metal in order to control the nominal oxygen stoichiometry. The samples were first intimately ground in an agate mortar and pressed in the form of bars. They were placed in evacuated quartz tubes and heated to 1200 °C at a heating rate of 200 °C·h^{-1}, held at this temperature for 24 h, and cooled to room temperature in 12 h.

The electron diffraction (ED) studies were carried out using a JEOL 2010 CX microscope fitted with an eucentric goniometer (±60°) and equipped with a liquid nitrogen holder. The high-resolution electron microscopy (HREM) images were recorded either with a JEOL 2011 FEG microscope equipped with a liquid nitrogen holder or with a TOPCON 002B microscope. HREM image calculations were carried out with the Mac-Tempas multislice program. The three microscopes operating at 200 kV were equipped with an energy dispersive spectroscopy (EDS) analyzer.

X-ray powder diffraction patterns were collected using a Philips X'pertPro diffractometer equipped with a secondary graphite monochromator working with the Cu Kα radiation. This system is equipped with an AntonPaar TTK450 chamber operating in the range from 100 to 723 K under nitrogen flow. Data were collected by step scanning over an angular range $5° \leq 2\theta \leq 100°$ and next were treated by profile analysis with the program Fullprof.[24]

Results

From the above experimental conditions, varying the nominal oxygen composition in the formula $Sr_3NdFe_3O_{10-x}$, a new phase, closely related to the $n = 3$ term $Sr_3LaFe_3O_{10}$ of the RP family,[21] is obtained for $1 < x \leq 1.5$. Nevertheless, the XRPD pattern (Figure 1a) of this black ceramic differs from that of $Sr_3LaFe_3O_{10}$ by the splitting of the [110] peak at $2\theta \approx 32.5°$ (enlargement Figure 1a), suggesting a rather large structural distortion with regard to the ideal tetragonal $n = 3$ RP. From the structural and thermogravimetric analyses, it will be shown further that three other new phases, related to the RP structure, are obtained in the hydrolysis/hydration dehydration process of $Sr_3NdFe_3O_{10-x}$.

The EDS and ED analyses carried out on numerous crystallites confirm that its actual cationic composition is "Sr_3NdFe_3", in the limit of accuracy of the technique. It must be emphasized that the as-synthesized $Sr_3NdFe_3O_{10-x}$ samples are unstable in air and react over several hours with ambient moisture, turning from black to brown and breaking up the bars. This feature is illustrated in Figure 1b by the growth of a peak at $2\theta \approx 5°$, implying a new periodicity close to 18 Å. This reactivity is all the more quick, since the nominal oxygen stoichiometry is close to 8.5 ($x = 1.5$). Redox titrations have been attempted from this limit compound to check the actual oxygen content. Thus, a stoichiometry close to 8.8 has been obtained; nevertheless, this value must be interpreted cautiously because the samples cannot be dissolved properly. So in the following parts, all oxygen stoichiometries are written from the nominal $O_{8.5}$ value.

I. The As-Synthesized Oxygen-Deficient RP Phase $Sr_3NdFe_3O_{9-\delta}$. The structural distortion of the as-synthesized $Sr_3NdFe_3O_{8.5}$ phase has been determined by electron diffraction. The sealed tube is opened just before preparing every grid, which is then quickly mounted on the sample holder and introduced in the microscope, so that the air exposure of the sample is only a few minutes.

Reconstructing the reciprocal space evidences a double cell with $a \approx a_p\sqrt{2}$, $b \approx a_p\sqrt{2}$ (a_p is the parameter of the perovskite unit cell), and $c \approx 28$ Å. No deviation from 90° has been detected between the main crystallographic axes. In the [001] ED patterns, a splitting of the spots occurs only in the $[110]_p$ direction, pointing to a small difference in length between the a and b parameters. This leads to the orthorhombic symmetry, in agreement with the XRPD observation. The reflection conditions hkl ($h + l = 2n$) and $0kl$ ($k, l = 2n$) are consistent with the space groups $Bbm2$ and $Bbmm$. Characteristic ED patterns are given in Figure 2.

Note that similar orthorhombic distortions are commonly observed in numerous perovskite relatives, strongly dependent on the cation size and oxidation states. One of the direct consequences of these phenomena is the formation of more or less large twinning domains. In the present oxide, they are easily detectable in the [001] ED patterns by the presence of a second system of weak extra spots (white arrows) along the direction perpendicular to a^* and also in the $[1\bar{2}0]/[2\bar{1}0]$ ED patterns by the fact that the $2h\ h\ l$ ($l = 2n$) and $h\ 2h\ l$ ($l = 2n + 1$) reflections are almost always present. Another consequence, less evident to detect, is that the [100] and [010] orientations are quite systematically superimposed. Bright field−dark field (BF−DF) imaging confirms that the twinning domain average width is a few tens of nanometers, as illustrated by the BF image in Figure 3 (the twin boundaries are indicated by white arrows). Moreover, these images systematically evidence drastic strain fields, which are similar to those observed in the $n = 1$ RP phases $Ca_{2-x}Ln_xMnO_4$.[5]

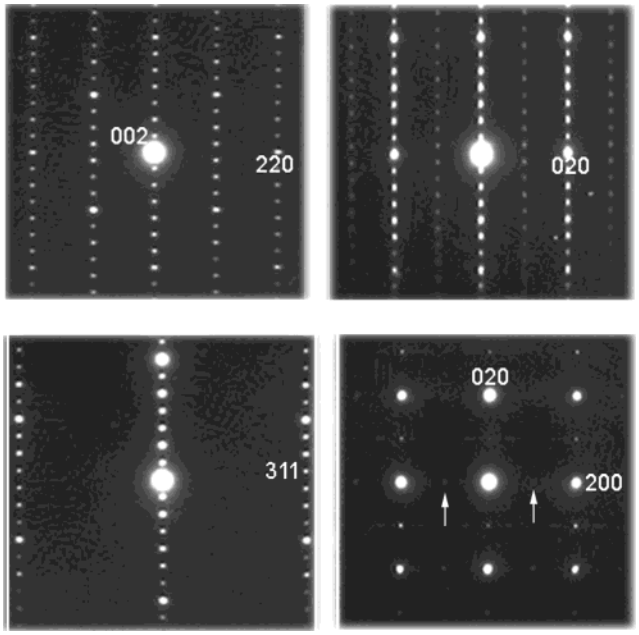

Figure 2. Experimental $[1\bar{1}0]$, [100], $[\bar{3}10]$, and [001] ED patterns of the as-synthesised $Sr_3NdFe_3O_{8.5}$.

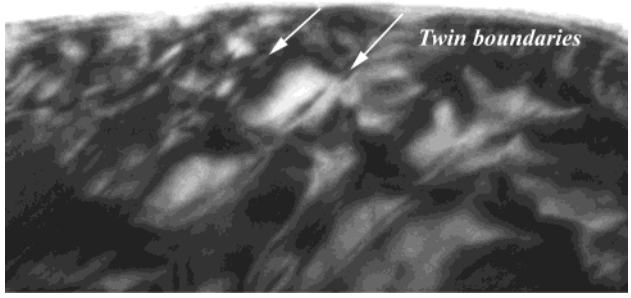

Figure 3. [001]-Oriented bright field image of the as-synthesized $Sr_3NdFe_3O_{8.5}$.

[110] is the best viewing direction for the characterization of the layer-stacking mode. The corresponding HREM images are in perfect agreement with an $n = 3$ RP-type structure. One example is given in Figure 4a, recorded with a defocus value close to −250 Å, where the high electron density zones appear as dark dots. The rock salt-type layers are imaged in the form of double rows of staggered dark dots, spaced by about 3.8 Å along $[1\bar{1}0]$ and 2.4 Å along [001]; two similar rows are observed in the perovskite block, associated with the (Sr,Nd) positions. The nature of the layers stacked along the c axis and the theoretical corresponding image, calculated for the refined positional parameters (Table 1) are given in Figure 4b. The very even contrast observed at the level of the different layers is remark-

(23) Yamura, K.; Huang, O.; Lynn, J. W.; Erwin, R. W.; Cava, R. J. *J. Solid State Chem.* **2000**, *152*, 374.
(24) Rodriguez-Carvajal, J. In *Collected abstract of powder diffraction meeting*; Galy, J., Ed.; 1990; p 127.

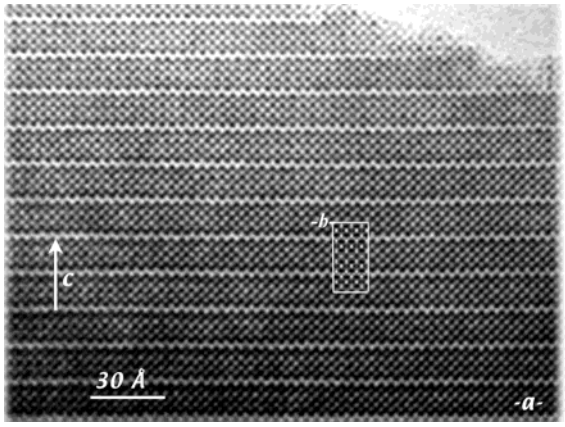

Figure 4. (a) Experimental [110] HREM image of as-synthesized $Sr_3NdFe_3O_{8.5}$ and (b) the corresponding simulated contrast calculated for a crystal thickness close to 35 Å and a defocus value $\Delta f = -250$ Å are inserted in the experimental image.

able. In the course of our investigation, a few $n = 1$ and 2 RP-type defective members have been detected, but the large majority of the crystallites are intergrowth defect free.

From these first TEM structural analyses, a model has been built considering a *Bbm*2 space group. All the reflections observed in the X-ray powder diffraction pattern (Figure 1) are indexed in this group with $a =$ 5.5196 (1) Å, $b =$ 5.4664 (1) Å, and $c =$ 28.750 (1) Å. The final refinement leading to a Bragg factor close to 0.115 is summarized in Table 1, where atomic positions are listed. The corresponding X-ray difference plot is shown in Figure 1. These calculations confirm the nature of the $n = 3$ RP-type structure and also show the presence of oxygen vacancies at the level of the basal plane [$FeO_{2-\delta}$] of the intermediate triple perovskite layer. No preferential occupation could be detected for the oxygen sites inside this [$FeO_{2-\delta}$] plane, but the low scattering factors of oxygen and the twinning phenomena evidenced by TEM techniques are not favorable factors.

Theoretically, the superstructure should be visible on the [010] HREM images, and the analysis of the through focus series could give information on its origin, such as cation ordering, oxygen/vacancy ordering as in the brownmillerite derivatives, or simply atomic displacements due to the tilting octahedra as in $GdFeO_3$.[23] The ordered contrast is indeed observed in the [010] HREM images but in fact disappears, unfortunately, very rapidly under the beam, resulting in an image contrast similar to that of the [100] images. This is exemplified in Figure 5a,b. In the [010] images (Figure 5a), the 5.52 Å periodicity along $\vec{a}$ is clearly observed, as the result of alternating bright and less bright spots; at $c/2 \approx 14.4$ Å along $\vec{c}$, this sequence is shifted by 2.76 Å along $\vec{a}$. The amplitude of the contrast variation is especially intense, for this focus value, at the level of the perovskite block. Such images can hardly be recorded, since the contrast is briefly observed and disappears before the through focus series is ended. Conversely, the HREM image given in Figure 5b exhibits an even contrast with double rows of bright dots, regularly spaced by 2.73 Å along $\vec{b}$. Therefore, the possibility cannot be excluded that the [100] image is a [010] image already "cleared" of the superstructure by the beam, before an image could be taken.

From this TEM study, no ordering has been detected between strontium and neodymium species. Taking into account the experimental defocus value, assumed to be close to −150 Å, and the high sensitivity to the electron beam, such contrasts are more likely associated with slight oxygen displacements at the level of the oxygen-deficient [$FeO_{2-\delta}$] basal plane of the iron polyhedra located in the middle of the perovskite block. This is in agreement with the theoretical images calculated for a statistical distribution of the oxygen vacancies in the basal plane of the medium iron "octahedra". As shown in Figure 5c, for focus values close to −150 Å, the tilt of

Table 1. Atomic Positions and Cell Parameters of $Sr_3NdFe_3O_{9-\delta}$ and Its Topotactic Derivatives

as-synthesized $Sr_3NdFe_3O_{9-\delta}$					$Sr_3NdFe_3O_{7.5}(OH)_2{\cdot}H_2O$					$Sr_3NdFe_3O_{7.5}(OH)_2$					$Sr_3NdFe_3O_{8.5}$				
atoms	*X*	*Y*	*Z*	*n*	atoms	*X*	*Y*	*Z*	*n*	atoms	*X*	*Y*	*Z*	*n*	atoms	*X*	*Y*	*Z*	*n*
Fe1	0.75	0.28	0	4	Fe1	0	0	0	2	Fe1	0	0	0	1	Fe1	0	0	0	2
Fe2	0.75	0.25	0.1429(5)	4	Fe2	0	0.1118(5)	0	4	Fe2	0	0	0.2413(8)	2	Fe2	0	0	0.1426(5)	4
Fe3	0.75	0.25	0.8572(5)	4	Sr1	0.5	0.0572(2)	0.5	3	Sr1	0.5	0.5	0.1257(4)	1.50	Sr1	0	0	0.5785(4)	3
Sr1	0.25	0.25	0.0784(3)	3	Nd1	0.5	0.0572(2)	0.5	1	Nd1	0.5	0.5	0.1257(4)	0.50	Nd1	0	0	0.5785(4)	1
Nd1	0.25	0.25	0.0784(3)	1	Sr2	0.5	0.1631(3)	0.5	3	Sr2	0.5	0.5	0.3575(4)	1.5	Sr2	0	0	0.7041(4)	3
Sr2	0.25	0.25	0.9216(3)	3	Nd2	0.5	0.1631(3)	0.5	1	Nd2	0.5	0.5	0.3575(4)	0.5	Nd2	0	0	0.7041(4)	1
Nd2	0.25	0.25	0.9216(3)	1	O1	0.5	0	0	2	O1	0.5	0	0	0.21	O1	0	0	0.197(1)	4
Sr3	0.25	0.25	0.2023(2)	3	O1b	0	0	0.5	2	O1′	0	0.5	0	0.89	O2	0	0.5	0.134(1)	6.25
Nd3	0.25	0.25	0.2023(2)	1	O2	0	0.052(5)	0	4	O2	0	0	0.102(2)	2	O3	0	0	0.059(1)	2.8
Sr4	0.25	0.25	0.7977(3)	3	O3	0.5	0.108(5)	0	4	O3	0.5	0	0.252(2)	2	O6	0.5	0	0	3.75
Nd4	0.25	0.25	0.7977(3)	1	O3b	0	0.892(5)	0.5	4	O3′	0	0.5	0.252(2)	2					
O1	0	0	0	1.50(9)	O4	0	0.189(4)	0	4	O4	0	0	0.405(2)	2					
O1b	0.5	0.55	0	2	OH1	0.5	0.2500	0	2	OH	0.288(9)	0.288(9)	0.500	1.4					
O2	0.74(6)	0.25	0.059(2)	4	OH2	0	0.7500	0.5	2										
O3	0.74(6)	0.25	0.941(2)	4															
O4	0	0	0.134(1)	3.1(9)															
O5	0.5	0.5	0.135(1)	3.4(9)															
O6	0.75	0.25	0.21061	4															
O7	0.75	0.25	0.78939	4															
O8	0	0	0.865(1)	3.1(9)															
O9	0.5	0.5	0.865(1)	3.4(9)															
*Bbm*2					*I*2/*m*					*Pmmm*					*I*4/*mmm*				
$a = 5.5196(4)$ Å					$a = 3.8910(6)$ Å					$a = 3.9054(7)$ Å					$a = 3.8926(5)$ Å				
$b = 5.4664(4)$ Å					$b = 35.500(8)$ Å					$b = 3.9087(8)$ Å					$b = 3.8926(5)$ Å				
$c = 28.745(1)$ Å					$c = 3.8910(6)$ Å					$c = 16.036(2)$ Å					$c = 28.721(3)$ Å				
$R_B = 0.115$					$\beta = 90.0(1)$					$R_B = 0.136$					$R_B = 0.125$				

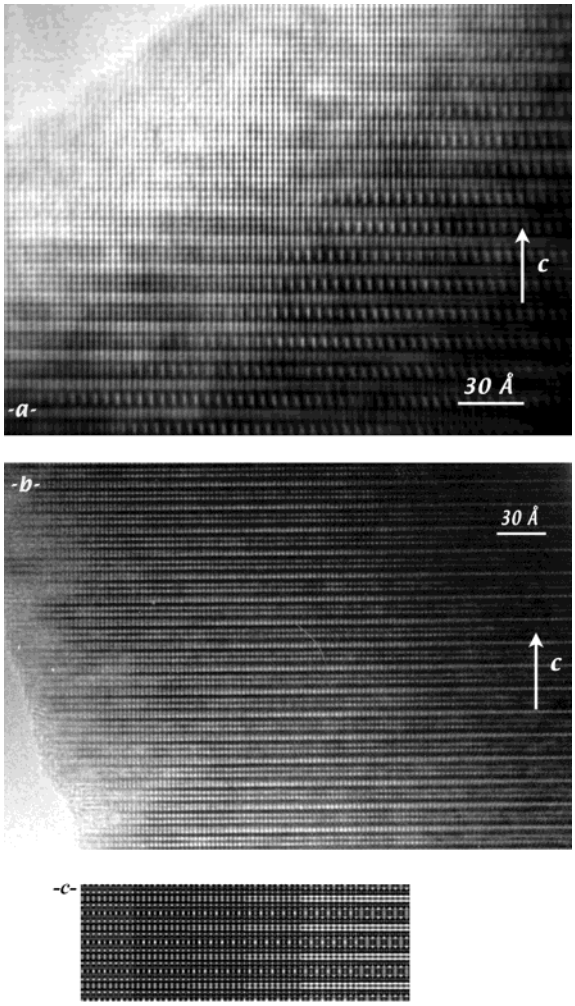

Figure 5. Experimental (a) [010] and (b) [100] HREM images of as-synthesized $Sr_3NdFe_3O_{8.5}$. (c) [010]-Oriented contrasts calculated with a thickness ranging from 15 to 100 Å and a defocus value $\Delta f = -150$ Å.

the octahedra is sufficient for generating the characteristic contrast of the superstructure, without any ordering of the oxygen atoms and vacancies.

II. Topotactic Reactions in the System $Sr_3NdFe_3O_{8.5}$·H_2O. The as-synthesized $Sr_3NdFe_3O_{8.5}$ phase is unstable in the presence of humidity. Its exposure to atmosphere moisture leads to a new phase in less than 24 h, characterized by a drastic change of the *c* parameter, as illustrated by the X-ray powder diffraction patterns shown in Figure 1b. The infrared characterizations have shown that this new phase contains H_2O molecules and OH groups, but no carbonate groups have been detected in the sample. The coupled thermodiffractometric (Figure 6) and thermogravimetric analysis (Figure 7), carried out up to 400 °C under nitrogen flow, shows that the new compound loses two H_2O molecules per formula in two steps. The first step takes place around 90 °C and can be attributed to the departure of one free water molecule, whereas the second step, corresponding to a second water molecule departure at about 250 °C, suggests that a dehydroxylation mechanism is engaged.

Thus, the new phase obtained by air exposure of the oxygen-deficient $Sr_3NdFe_3O_{8.5}$ phase can be considered as the result of a hydration−hydrolysis reaction according to the equation:

$$Sr_3NdFe_3O_{8.5} + 2H_2O \rightarrow Sr_3NdFe_3O_{7.5}(OH)_2{\cdot}H_2O$$

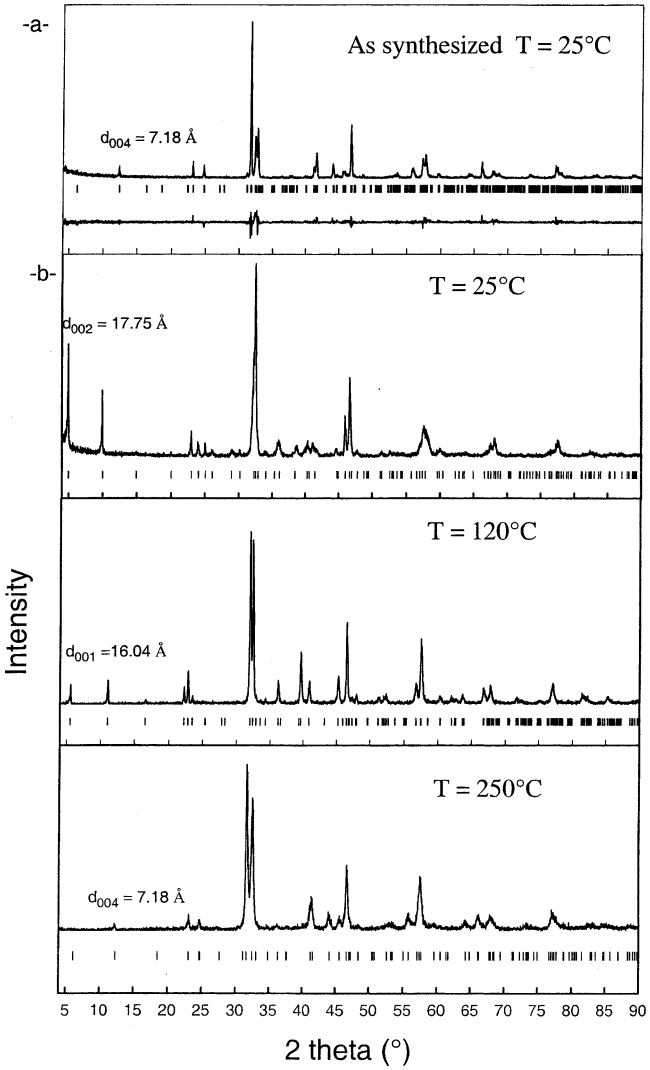

Figure 6. (a) Experimental XRD pattern and difference plot of the as-synthesized $Sr_3NdFe_3O_{8.5}$ at room temperature. (b) XRD patterns of its oxy-hydroxide hydrated $Sr_3NdFe_3O_{7.5}(OH)_2{\cdot}H_2O$ at $T = 25$ °C and its evolution versus temperature. Vertical bars are the Bragg angle positions for the *I*2/*m* ($T = 25$ °C), *Pmmm* ($T = 120$ °C), and *I*/4*mmm* ($T = 250$ °C) space groups.

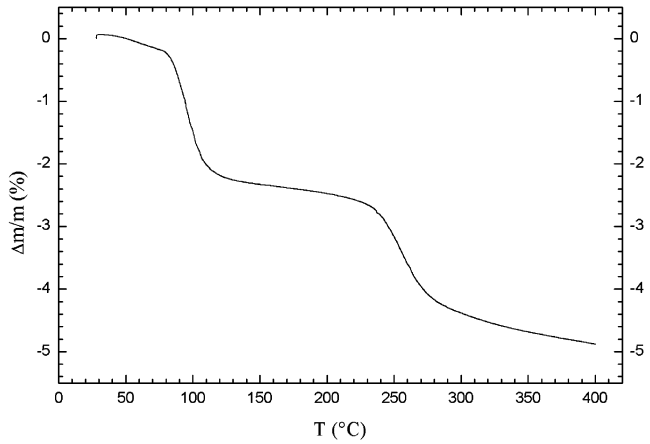

Figure 7. TGA pattern of the oxy-hydroxy hydrate $Sr_3NdFe_3O_{7.5}(OH)_2{\cdot}H_2O$ collected under nitrogen flow.

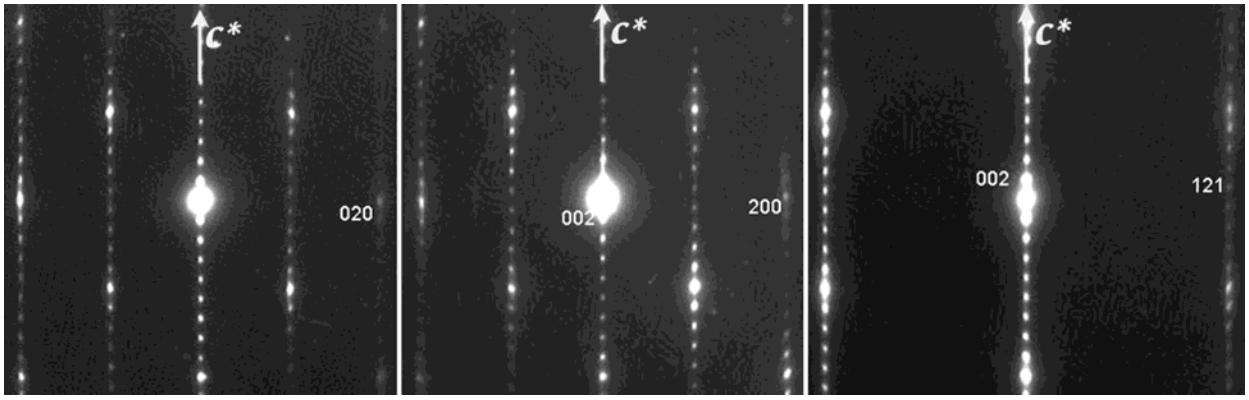

Figure 8. Experimental ED patterns of the oxy-hydroxy hydrate $Sr_3NdFe_3O_{7.5}(OH)_2{\cdot}H_2O$.

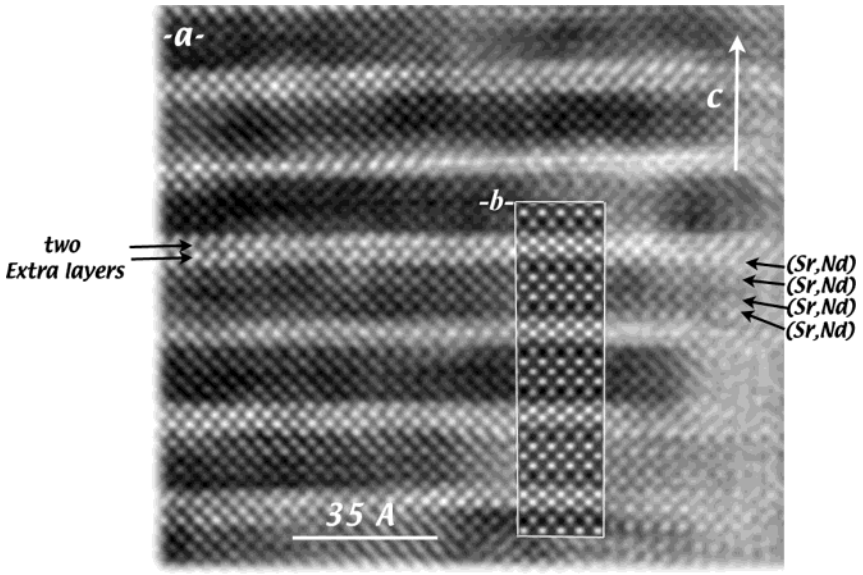

Figure 9. Experimental (a) and simulated (b) [100] HREM images of the oxy-hydroxyde hydrate $Sr_3NdFe_3O_{7.5}(OH)_2{\cdot}H_2O$ calculated for a crystal thickness close to 39 Å and a defocus value $\Delta f = -900$ Å.

Keeping the thermogravimetric analysis in mind, it clearly appears that the decomposition of hydrated $Sr_3NdFe_3O_{7.5}(OH)_2{\cdot}H_2O$ phase occurs in two steps and leads first to the formation of the oxy-hydroxide, $Sr_3NdFe_3O_{7.5}(OH)_2$, phase and finally to the oxide $Sr_3NdFe_3O_{8.5}$, according to the equations

$$Sr_3NdFe_3O_{7.5}(OH)_2{\cdot}H_2O \xrightarrow{T > 80\ ^\circ C} Sr_3NdFe_3O_{7.5}(OH)_2 + H_2O\uparrow \xrightarrow{T > 250\ ^\circ C} Sr_3NdFe_3O_{8.5} + H_2O\uparrow$$

Structural Characterization of the Oxy-Hydroxide Hydrate $Sr_3NdFe_3O_{7.5}(OH)_2{\cdot}H_2O$. The XRPD pattern of this hydrated phase (Figure 6) evidences close structural relationships with that of $Sr_3NdFe_3O_{8.5}$ but clearly shows that it does not belong to the classical RP series. It is indexed in a monoclinic cell with $a = 3.891(1)$ Å, $b = 3.891(1)$ Å, $c = 35.508(1)$ Å, $\beta = 90.0(1)°$, in agreement with the ED study. Due to the low stability under vacuum at room temperature, this phase cannot be observed in the electron microscope at room temperature, since it suffers structural changes in a few minutes, transforming into $Sr_3NdFe_3O_{7.5}(OH)_2$ by progressive loss of one water molecule. The electron diffraction study of this hydrate was then carried out at 92 K, using a $N_2(l)$ cooling sample holder and spreading the beam at the maximum. The reconstruction of the reciprocal space evidences a monoclinic cell with $a \approx 3.9$ Å, $b \approx 3.9$ Å, $c \approx 35.5$ Å, $\beta = 90° + \epsilon°$. The reflection condition is hkl ($h + k + l = 2n$), compatible with the space groups $I2/m$ and $I2$. The monoclinic distortion is small but is clearly evidenced by superposing the [001] electron diffraction patterns directly, thus excluding any possible errors due to the measuring process. Three characteristic ED patterns are given in Figure 8. The elongated shape of the reflections shows a rather poor crystalline quality due the metastability of the hydrate and microtwinning phenomena due to the monoclinic distortion.

Accurate HREM images of the $Sr_3NdFe_3O_{7.5}(OH)_2{\cdot}H_2O$ phase are hardly recordable under these conditions, and even less for a complete focus series; they all evidence the local formation of $Sr_3NdFe_3O_{7.5}(OH)_2$ and suffer from the transition steps. An example of the [100] image quickly recorded at 100 K is given in Figure 9a. The low electron density areas are highlighted and the typical arrangement of the gray and dark spots is typical of structural units built up of three perovskite-type layers. These perovskites slices are separated by three or four rows of staggered, very bright dots, the number

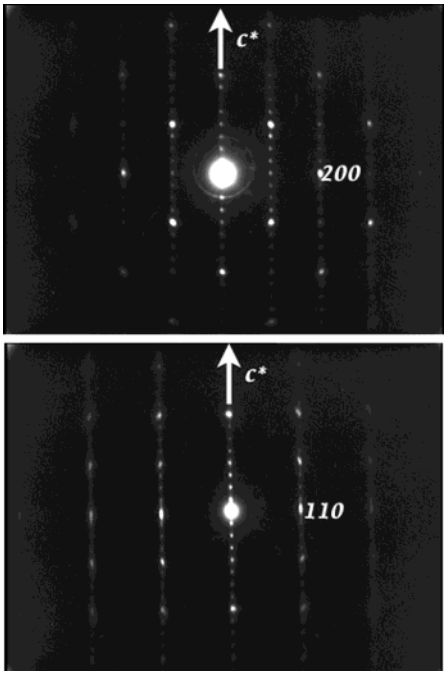

Figure 10. Experimental [010] and [1$\bar{1}$0] ED patterns of the oxy-hydroxide $Sr_3NdFe_3O_{7.5}(OH)_2$.

and spacing of these rows locally varying. The 17.75 Å periodicity ($c/2$) is related to the hydrated oxy-hydroxide $Sr_3NdFe_3O_{7.5}(OH)_2{\cdot}H_2O$. Despite the large distortion and complex phenomena that locally affect the contrast at the level of the four bright rows, these images reveal some important information. First, it clearly appears that the sequence of the (Sr/Nd) and Fe layers is unchanged, so one can conclude that the structural change does not affect directly the perovskite block. The four rows of brighter dots can be interpreted by the intercalation of two extra layers between the two rock salt-type [(Sr,Nd)O] layers of the as-synthesized $Sr_3NdFe_3O_{8.5}$ framework. The two [(Sr,Nd)O] layers correspond to each other by a double translation $\vec{t} \approx (2.75 + 3.4)$ Å along $\vec{c}$ (2.75 Å is the thickness of the rock salt layer and 3.4 Å is the amplitude of the displacement due to the intercalated layers) and $1/2\vec{a} + 1/2\vec{b}$ in the (001) plane, in agreement with the *I*-type symmetry. On the basis of a hydration/hydrolysis reaction and the observation of the double extra rows between the rock salt layers, a structural model can be proposed for $Sr_3NdFe_3O_{7.5}(OH)_2{\cdot}H_2O$. Taking into account the poor crystalline quality, it is unrealistic to refine temperature factors and especially positions of H_2O/OH groups from X-ray diffraction data. Consequently, B factors have been fixed to 0.5 and 1 for cationic and anionic sites, respectively, while H_2O/OH groups have been idealized as "oxygen" site. The hydrolysis reaction would likely be statistically located at the level of the rock salt layer, forming Sr−OH bonds as in $Sr(OH)_2$, $Sr(OH)_2{\cdot}H_2O$, or $Sr(OH)_2{\cdot}8H_2O$[25] and Fe−OH bonds as in the ReO_3-type structure of $Fe(OH)_3$.[26] It is schematically drawn in Figure 14, where the hatched circles are the (Sr/Nd) atoms and the gray circles the oxygen atoms of the hydroxyl groups, while the water molecules are model-

(25) Buchmeier, W.; Lutz, H. D. *Z. Anorg. Allg. Chem.* **1986**, *538*, 131.
(26) Okamoto *J. Am. Ceram. Soc.* **1968**, *51*, 54.

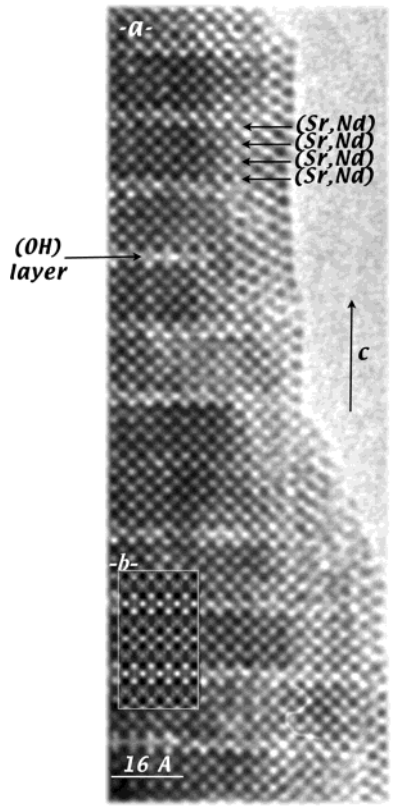

Figure 11. Experimental (a) and simulated (b) [100] HREM images of the oxy-hydroxy $Sr_3NdFe_3O_{7.5}(OH)_2$ calculated with a thickness close to 39 Å and a defocus value $\Delta f = -250$ Å.

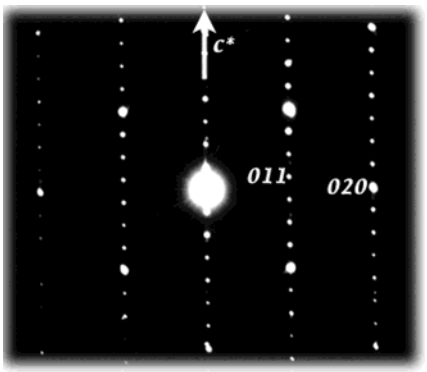

Figure 12. Experimental [100] ED patterns of the dehydrated $Sr_3NdFe_3O_{8.5}$ phase.

ized as black circles. The calculated images with the ideal model given in positions Table 1 fit with the experimental ones, as shown in Figure 9b, where the light electron density zones are highlighted (focus −900 Å and crystal thickness 39 Å). Nevertheless, neutron diffraction data are absolutely necessary to validate definitely such a model.

Structural Characterization of the Oxy-Hydroxide $Sr_3NdFe_3O_{7.5}(OH)_2$. Working at room temperature by TEM techniques, most of the crystallites exhibit a different structure, the parameters of which are in agreement with those determined from the XRPD pattern collected at 120 °C (Figure 6). The reconstruction of the reciprocal space reveals a primitive cell with $a \approx b \approx 3.9$ Å, $c \approx 16$ Å, and $\alpha, \beta, \gamma = 90°$. There are no conditions limiting the reflections. The [100] and [110] ED patterns are given in Figure 10. The cell parameters

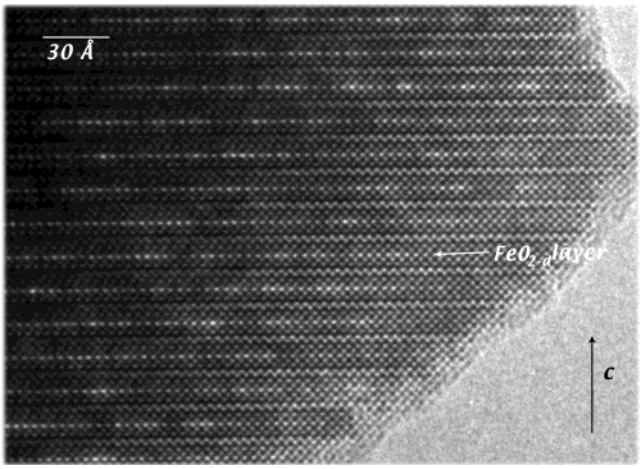

Figure 13. Experimental [100] HREM image of the dehydrated $Sr_3NdFe_3O_{8.5}$ phase.

were refined in *Pmmm* from XRPD data to $a = 3.905(1)$ Å, $b = 3.909(1)$ Å, and $c = 16.036(2)$ Å.

The HREM $[100]_p$ oriented image in Figure 11a has been recorded with a defocus value where the low electron density rows are highlighted. One also observes that the triple perovskite layers remain unchanged and that a single extra layer remains inserted between the [(Sr,Nd)O] layers, which are simply translated by $\vec{t} \approx (2.75 + 1.7)$ Å along $\vec{c}$, loosing the translation $1/2\vec{a} + 1/2\vec{b}$ in the (001) plane, in agreement with the *P*-type symmetry. Note that the contrasts of the HREM images, for different focus values, can be compared to those observed for the copper oxycarbonates, where a very close spacing and a similar loss of symmetry is induced by the insertion of the carbonate groups between two [AO] layers.[27] Following the proposed mechanism, an idealized model can be drawn (Figure 14) for the rock salt layers of $Sr_3NdFe_3O_{7.5}(OH)_2$ structure, one OH layer being sandwiched between two SrO layers. Considering these TEM structural analyses, a model has been built considering the *Pmmm* space group, and the Fourier differences map sections calculated at the level of the

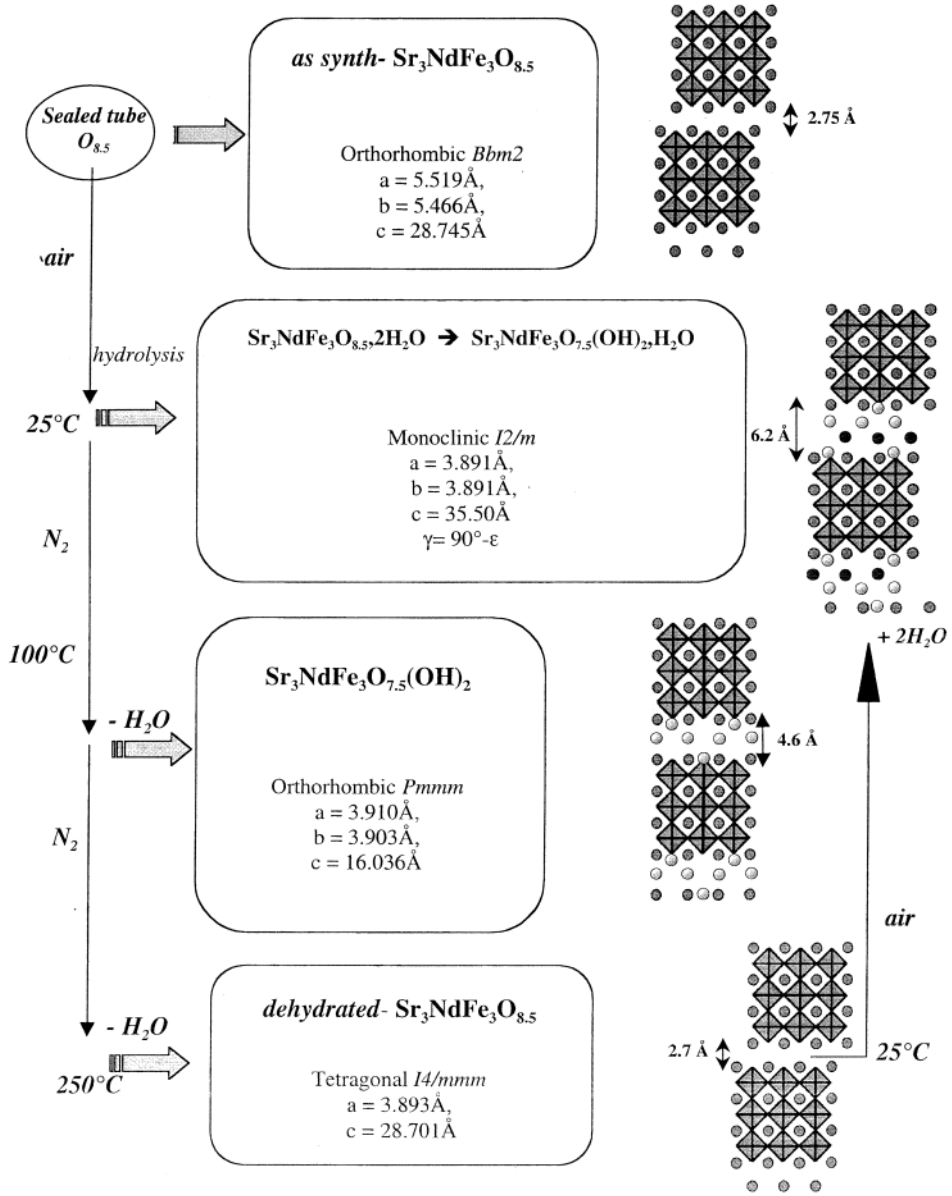

Figure 14. Structural mechanism and stacking mode of the different phases. Water molecules and hydroxyl groups are idealized as black and gray circles, respectively.

inserted layer evidence electron density in positions close to (0.3, 0.3, 0.5). All the reflections observed in the powder X-ray diffraction pattern (Figure 6) are indexed in the orthorhombic cell. The final refinement is summarized in Table 1 with the atomic positions. Since these calculations lead to a R_{Bragg} factor close to 0.13, the corresponding positional parameters allow through focus theoretical HREM series to be calculated (Figure 11b), fitting with the experimental ones.

Structural Characterization of the Dehydrated Phase. Finally, the XRPD pattern of the sample collected at 250 °C under nitrogen flow (Figure 6), after $2H_2O$ departure, is very similar to that of the as-synthesized phase, except that the splitting of the [110] reflection is not observed. After complete dehydration, the sample was cooled to room temperature under nitrogen flow and maintained in this atmosphere until the parameters are stabilized, and then the sample for TEM study was freshly prepared, the thermodiffractometric analyses showing that under these conditions no significant rehydration is observed. The reconstruction of the reciprocal space shows a tetragonal cell, and the reflection conditions are compatible with the *I*4/*mmm* space group, as illustrated by the ED [100] pattern shown in Figure 12. The [100] HREM image (Figure 13) confirms the $n = 3$ RP-type structure, with a single rock salt layer intergrown with a triple perovskite layer. The cell parameters were refined at $a = 3.8926(5)$ Å and $c = 28.721$ (3) Å, and the positional parameters are given in the Table 1.

In that way, the as-synthesized and dehydrated $Sr_3NdFe_3O_{8.5}$ phases are both an $n = 3$ member of the RP series, with very close parameters, and they only differ by the symmetry, the first one being strongly distorted, whereas the latter exhibits almost the ideal symmetry. Several hypotheses could be put forward for explaining these differences, accounting for differences in pressure, temperature, or the presence of OH groups, but all of them need a lot of complementary heavy experiments to be tested. At the present state of the work, apart from the symmetry, the main difference in the HREM images is observed at the level of the oxygen-deficient [$FeO_{2-\delta}$] layer of the iron polyhedra located in the middle of the perovskite block (compare Figures 4 and 13). The contrast is less regular with irregular brightness of the dots. Even if these contrast modulations do not show up on any Fourier transforms of the images, they suggest local atomic displacements in an average structure.

Structural Mechanism. The topotactic nature of the reactions that take place during the hydrolysis/hydration of $Sr_3NdFe_3O_{9-\delta}$ is easily understood by comparing the different structures of the above compounds. The four reactions of synthesis and hydrolysis/hydration cycle of $Sr_3NdFe_3O_{9-\delta}$ are thus summarized in Figure 14 in which the corresponding structures are schematically drawn. Starting from the as-synthesized, oxygen-deficient RP oxide $Sr_3NdFe_3O_{9-\delta}$, the hydration/hydrolysis reaction occurs topotactically at room temperature with the insertion of two additional [OH] and [H_2O] layers between the [Nd/SrO] layers building the RS-type layer. Such an intercalation implies an *I*-type symmetry in the hydrated oxy-hydroxy $Sr_3NdFe_3O_{7.5}(OH)_2 \cdot H_2O$ structure. By the departure of one H_2O molecule, a gliding of the perovskite block is observed, leading to a *P*-type symmetry of the oxy-hydroxy $Sr_3NdFe_3O_{7.5}(OH)_2$. Last, this complete dehydration process under nitrogen flow leads to an $n = 3$ RP structure, which is highly moisture sensitive as well. The reversibility of these reactions is also in perfect agreement with their topotactic character. The latter feature is clearly supported by examining numerous crystallites for which an equilibrium is not reached, as the result of either an unachieved reaction or the metastability of the phase under the electron beam. An example is given in Figure 15, where the three structural types coexist, stacked along $\vec{c}$, within the same crystallite. The double [Nd/SrO] layers of the $n = 3$ RP structure are indicated by a single arrow, the double [Nd/SrO] layers plus the extra layer of $Sr_3NdFe_3O_{7.5}(OH)_2$ by a double arrow, and, last, the double [Nd/SrO] layers plus the two extra layers of $Sr_3NdFe_3O_{7.5}(OH)_2 \cdot H_2O$ by a triple arrow. This image clearly evidences the translation of the perovskite building blocks. In that example, the different steps of the cycle appear as intergrowth members for which both the periodicity and cell symmetry are involved, explaining the diffuse lines sometimes observed along c^* in any [*hk*0] ED patterns.

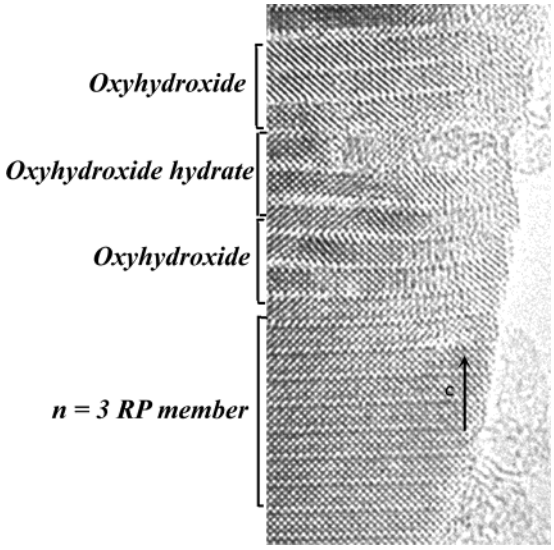

Figure 15. Experimental [100] HREM image showing that $Sr_3NdFe_3O_{9-\delta}$ and its topotactic derivatives can coexist inside the same crystallite.

Concluding Remarks. A new oxygen-deficient $Sr_3NdFe_3O_{9-\delta}$ oxide, exhibiting an $n = 3$RP-type structure has been isolated, in which the oxygen vacancies are mainly located at the level of the intermediate [$FeO_{2-\delta}$] layer. The XRPD refinement of the occupation sites allows only concluding that the perovskite block is oxygen-deficient, but neutron diffraction data analyses are absolutely necessary for an accurate determination of the oxygen/vacancies content and their distribution. This compound is very labile and topotactically transforms into oxy-hydroxyde hydrate $Sr_3NdFe_3O_{7.5}(OH)_2 \cdot H_2O$ in moist air. The XRPD study of the reactivity of the system has shown that the dehydrated phase, obtained after a thermal cycle up to 673 K under nitrogen flow, has kept the same ability to react with the ambient atmosphere. Exposure again to air for 12

(27) Babu, T. G. N.; Fish, D. J.; Greaves, C. *J. Mater. Chem.* **1991**, *1*, 677.

h induces its transition back to $Sr_3NdFe_3O_{7.5}(OH)_2 \cdot H_2O$, showing that the hydration/dehydration mechanism, summarized in Figure 14, is reversible. The preliminary study carried out for following in situ the dehydration mechanism by electron microscopy, heating the sample at 250 °C, showed that the reaction is not yet engaged after a few hours, suggesting that the hydrogen bonds, which are assumed to stabilize the framework, are rather strong.

This study confirms the possibility to stabilize oxygen-deficient RP-type iron oxides. More importantly, it demonstrates the extraordinary flexibility of this structural framework, whose rock salt layers are able to intercalate and deintercalate extra [OH] and [H_2O] layers. This ability of layered structures to accommodate foreign species has previously been observed in cuprates such as $Sr_2Cu(CO_3)O_2$[27] or $IBi_{2n}Sr_{2n}Ca_nCu_{2n}O_x$,[28] in titanates such as $H_2Nd_2Ti_3O_{10} \cdot xH_2O$,[29] and in tantalates such as $K_2SrTa_2O_7 \cdot xH_2O$,[30] where carbonate groups, halogenures species, or H_2O molecules can be introduced between perovskite layers. The present compounds differ from all the other ones by the quite reversible, simultaneous character of the intercalation reactions with hydrolysis. In this respect, the dehydroxylation reaction that appears for $Sr_3NdFe_3O_{7.5}(OH)_2$ can be compared with the one observed for the FeO(OH) goethite → Fe_2O_3 hematite transformation.[31] Both reactions are topotactic, but for the present phase the reaction is reversible at room temperature, in contrast to that of hematite.

These results illustrate the richness of the intercalation mechanisms in the layered structures. The possibility to intercalate water molecules in an RP-type framework opens a multistep, low-temperature route to isolate new materials by means to hydration/dehydration mechanisms.

Acknowledgment. The authors are grateful to Prof. M. Daturi, for the infrared characterizations and the fruitful discussions, and M. Lozier, for the collection of X-ray diffraction data.

CM030351N

(28) Kijima, N.; Gonsky, R.; Xiang, X. D.; Vareka, W. A.; Zettl, A.; Corkill, J. L.; Cohen, M. L. *Physica C* **1992**, *597*, 190.
(29) Richard, M.; Brohan, L.; Tournoux, M. *J. Solid State Chem.* **1994**, *112*, 345.
(30) Kodenkandath, T. A.; Wiley, J. B. *Mater. Res. Bull.* **2000**, *35*, 1737.
(31) Watari, F.; Van Lanuydt, J.; Delavignette, P.; Amelinckx, S. *J. Solid State Chem.* **1979**, *29*, 137.